

Anomalous magnon Nernst effect of topological magnonic materials

X S Wang^{1,2} and X R Wang^{2,3,*}

¹*School of Microelectronics and Solid-State Electronics,
University of Electronic Science and Technology of China, Chengdu, Sichuan 610054, China*

²*Department of Physics, The Hong Kong University of Science and Technology,
Clear Water Bay, Kowloon, Hong Kong*

³*HKUST Shenzhen Research Institute, Shenzhen 518057, China*

The magnon transport driven by thermal gradient in a perpendicularly magnetized honeycomb lattice is studied. The system with the nearest-neighbor pseudodipolar interaction and the next-nearest-neighbor Dzyaloshinskii-Moriya interaction (DMI) has various topologically nontrivial phases. When an in-plane thermal gradient is applied, a transverse in-plane magnon current is generated. This phenomenon is termed as the anomalous magnon Nernst effect that closely resembles the anomalous Nernst effect for an electronic system. The anomalous magnon Nernst coefficient and its sign are determined by the magnon Berry curvatures distribution in the momentum space and magnon populations in the magnon bands. We predict a temperature-induced sign reversal in anomalous magnon Nernst effect under certain conditions.

PACS numbers: 75.30.Ds,75.30.Sg

Keywords: magnon, topology, Berry curvature, Nernst effect

* Corresponding author:phxwan@ust.hk

I. INTRODUCTION

Spintronics is about generation, detection and manipulation of spin degree of freedom of particles. Most early studies focused on the electron spins [1]. However, an electric current normally accompanies an electron spin current and consumes much energy, leading to a Joule heating. The Joule heating becomes the critical problem in nano electronics and spintronics although many efforts have been made. Recently, magnon spintronics, or magnonics in which magnons are spin carriers, attracts much attention because of its fundamental interest [2, 3] and its lower energy consumption in comparison with that of electron spintronics [4–6].

Nernst effect commonly refers to the generation of a transverse voltage/current by a thermal gradient in an electronic system under a perpendicular magnetic field. In a ferromagnetic metal and in the absence of an external magnetic field, a thermal gradient can generate a transverse charge current or voltage proportional to the vector product of the thermal gradient and the magnetization in the linear response region. This is the anomalous Nernst effect, the thermal electric manifestation of the anomalous Hall effect [7]. It is natural to ask whether there is a similar effect for magnons. Moving magnons experience gyroscopic forces because of nonzero Berry curvature of a magnetic system although magnons are charge neutral quasiparticles that do not have the Lorentz force. As a result, a transverse magnon current is generated when magnons are driven by a longitudinal force such as a thermal gradient in the absence of a magnetic field which is termed as the anomalous magnon Nernst effect (AMNE). In this paper, we focus on a perpendicularly magnetized honeycomb lattice with the nearest-neighbor pseudodipolar interaction and the next-nearest-neighbor Dzyaloshinskii-Moriya interaction (DMI), whose magnon bands can be topologically nontrivial with various topological phases [8]. We investigate the magnon transport of this system in the presence of a thermal gradient using the semiclassical equations of motion of magnons and the Boltzmann equation in linear transport regime. We found that the system has topologically nontrivial magnon bands. The system changes from one topologically nontrivial phase to another as the DMI strength varies. The AMNE coefficient depends on temperature nonmonotonically. It starts from 0 at 0 K and goes back to 0 at high temperature limit with a maximum at an intermediate temperature. The nonmonotonic temperature-dependence of AMNE is due to non-trivial Berry curvature distribution of a given band in the momentum space and thermally activated magnon population in the

bands. In certain parameter space, there is a sign reversal of the AMNE at low temperature because the magnon Berry curvature near the band bottom at Γ point has small non-zero values of the opposite sign as those near band top at K and K' points with a much bigger value. In the presence of staggered anisotropy on A, B sublattices, the system can also be topologically trivial, and the K and K' valleys contribute opposite transverse magnon currents due to the opposite Berry curvatures. However, the total transverse magnon current does not vanish. The boundary that AMNE coefficient changes its sign is also determined numerically.

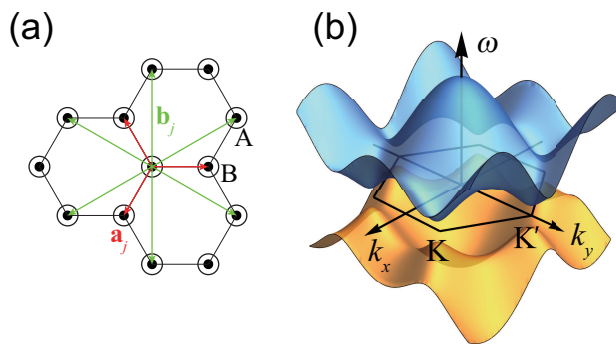


FIG. 1. (a) Schematic illustration of a perpendicularly magnetized honeycomb lattice. The red and green arrows denote the nearest-neighbor and the next-nearest-neighbor vectors, respectively. (b) Magnon spectrum $\omega(\mathbf{k})$ of an infinite system for $K = 10J$, $F = 5J$, and $D = \Delta = 0$. The Brillouin zone is indicated by the black hexagon.

II. MODEL AND RESULTS

We consider classical magnetic moments on a honeycomb lattice in the xy plane as illustrated in Figure 1(a), and the Hamiltonian is

$$\mathcal{H} = -\frac{J}{2} \sum_{\langle i,j \rangle} \mathbf{m}_i \cdot \mathbf{m}_j - \frac{F}{2} \sum_{\langle i,j \rangle} (\mathbf{m}_i \cdot \mathbf{e}_{ij})(\mathbf{m}_j \cdot \mathbf{e}_{ij}) - D \sum_{\langle\langle i,j \rangle\rangle} \nu_{ij} \hat{\mathbf{z}} \cdot (\mathbf{m}_i \times \mathbf{m}_j) - \sum_i \frac{K_i}{2} m_{iz}^2, \quad (1)$$

where the first term is the nearest-neighbor ferromagnetic Heisenberg exchange interaction ($J > 0$). The second and third terms arise from the spin-orbit coupling (SOC) [9, 10]. \mathbf{e}_{ij} is the unit vector pointing from site i to j . F is the strength of the nearest-neighbor

pseudodipolar interaction, which is the second-order effect of the SOC [The nearest-neighbor Dzyaloshinskii-Moriya interaction (DMI) would be the first-order effect of SOC if it exists, but it vanishes because the center of the A-B bond is an inversion center of the honeycomb lattice]. The next-nearest-neighbor DMI measured by D is in general no zero. $\nu_{ij} = \frac{2}{\sqrt{3}}\hat{\mathbf{z}} \cdot (\mathbf{e}_{li} \times \mathbf{e}_{lj}) = \pm 1$, where l is the nearest neighbor site of i and j . The last term is the sublattice-dependent anisotropy whose easy-axis is along the z direction with anisotropy coefficients of $K_i = K + \Delta$ for $i \in A$ and $K - \Delta$ for $i \in B$. \mathbf{m}_i is the unit vector of the magnetic moment at site i . The spin dynamics is governed by the Landau-Lifshitz-Gilbert (LLG) equation [8, 12],

$$\frac{d\mathbf{m}_i}{dt} = -\gamma \mathbf{m} \times \mathbf{H}_i^{\text{eff}} + \alpha \mathbf{m}_i \times \frac{d\mathbf{m}_i}{dt}, \quad (2)$$

where γ is the gyromagnetic ratio and α is the Gilbert damping constant. $\mathbf{H}_i^{\text{eff}} = \frac{\partial \mathcal{H}}{\mu_0 \mu \partial \mathbf{m}_i}$ is the effective field at site i . The lattice constant a and J are used as the length unit and the energy unit out of five parameters in (1). The magnetic field and time are in the units of $\sqrt{J\mu_0/a^3}$ and $\sqrt{a^3\mu_0/(J\gamma^2)}$, respectively, where μ_0 is the vacuum permeability. When the anisotropy is sufficiently large, spins are perpendicularly magnetized [13]. To obtain the spin wave spectrum, we linearize the LLG equation following the standard procedures [8]. The spin wave spectrum and wavefunctions are obtained by solving the eigenvalue problem $gH(\mathbf{k})\psi_n = \omega_n(\mathbf{k})\psi_n$, where $H(\mathbf{k})$ is a 4×4 Hermitian matrix

$$H = \begin{pmatrix} M_A^+ & 0 & -\ell(\mathbf{k}) & -g_+(\mathbf{k}) \\ 0 & M_A^- & -g_-(\mathbf{k}) & -\ell(\mathbf{k}) \\ -\ell^*(\mathbf{k}) & g_-^*(\mathbf{k}) & M_B^- & 0 \\ -g_+^*(\mathbf{k}) & \ell^*(\mathbf{k}) & 0 & M_B^+ \end{pmatrix}, \quad (3)$$

with $\ell(\mathbf{k}) = (J + \frac{F}{2}) \sum_{j=1,2,3} e^{i\mathbf{k} \cdot \mathbf{a}_j}$, $g_{\pm}(\mathbf{k}) = \frac{F}{2} \sum_{j=1,2,3} e^{\pm 2i\theta_j} e^{i\mathbf{k} \cdot \mathbf{a}_j}$ (θ_j is the angle between \mathbf{a}_j and x direction). $M_A^{\pm} = M + \Delta \pm d(\mathbf{k})$ and $M_B^{\pm} = M - \Delta \pm d(\mathbf{k})$ with $M = K + 3J$ and $d(\mathbf{k}) = 2D \sum_{j=1,3,5} \sin(\mathbf{k} \cdot \mathbf{b}_j)$. $g = \sigma_0 \otimes \sigma_3$ (with σ_0 being the 2×2 identity matrix and σ_3 the Pauli matrix). ψ_n is the n th eigenvector of eigen-frequency ω_n , satisfying the generalized orthogonality $\psi_i^\dagger g \psi_j = \delta_{ij}$. At K and K' , the frequencies of the two magnon bands are respectively,

$$\omega_1^{K(K')} = M - 3\sqrt{3}D + (-)\Delta, \quad (4)$$

$$\omega_2^{K(K')} = \sqrt{(M + 3\sqrt{3}D)^2 - \frac{9}{4}F^2} - (+)\Delta, \quad (5)$$

where “(+)” and “(-)” on the right hand side are for K' . The magnon band for $K = 10J$, $F = 5J$ and $D = \Delta = 0$ is shown in Figure 1(b), which has a direct gap of $\Delta_g = M - \sqrt{M^2 - 9F^2/4}$ at both K and K' (valleys for the upper band and peaks for the lower band). The direct gap at the valleys can close and reopen as D and Δ varies, resulting in topological phase transitions. The Berry curvature $\mathbf{\Omega}_n$ of n th band and the corresponding Chern number \mathcal{C}_n can be calculated by using a gauge-invariant formula [16],

$$\mathbf{\Omega}_n = i\nabla_{\mathbf{k}} \times (\psi_n^\dagger g \nabla_{\mathbf{k}} \psi_n); \quad (6)$$

$$\mathcal{C}_n = \frac{1}{2\pi} \iint_{\mathbf{k} \in \text{BZ}} \Omega_n d^2\mathbf{k}, \quad (7)$$

where the integration is over the Brillouin zone (BZ), and $\Omega_n = \mathbf{\Omega}_n \cdot \hat{\mathbf{z}}$ is the z component of the Berry curvature that is given by a gauge-invariant formula similar to that in electronic systems [15]

$$\mathbf{\Omega}_n = i\text{Tr} \left[P_n \left(\frac{\partial P_n}{\partial k_x} \frac{\partial P_n}{\partial k_y} - \frac{\partial P_n}{\partial k_y} \frac{\partial P_n}{\partial k_x} \right) \right] \hat{\mathbf{z}}, \quad (8)$$

where P_n is the projection matrix of the n th band defined as $P_n = \psi_n \psi_n^\dagger g$.

Figure 2(a) is the phase diagram in $D/J - \Delta/J - F/J$ space for $K = 10J$. The various topological phases are classified by Chern numbers \mathcal{C}_l and \mathcal{C}_u of lower and upper magnon bands. $\mathcal{C}_l + \mathcal{C}_u = 0$ satisfies the “zero sum rule” [15, 17]. The magnon band Chern number change its value when magnon band gap closes and reopens at valley K or K' . Thus, the band gap closing at K or K' defines two phase boundary surfaces of $\omega_1^{K'} = \omega_2^{K'}$ and $\omega_1^K = \omega_2^K$ (See Eqs. (4) and (5)). For convenience, we define

$$\Delta_c = \frac{1}{2} \left[\sqrt{(M + 3\sqrt{3}D)^2 - \frac{9}{4}F^2} - (M - 3\sqrt{3}D) \right], \quad (9)$$

and two phase boundary surfaces are $\Delta = \pm\Delta_c$, denoted as the orange surfaces. They divide the whole space into four regions. In the region of $\Delta_c < 0$ and $\Delta_c < \Delta < -\Delta_c$, \mathcal{C}_u is 1. The density plot of Ω for $F = 5J$, $\Delta = D = 0$ (O_1 in Fig. 2(a)) is shown in the top panel of Fig. 2(b). Interestingly, the lower band has two contour curves of $\Omega = \Omega_l = 0$ around Γ denoted by black dash lines. The two contour curves divide the first Brillouin zone into three parts. Ω is slightly positive inside the inner contour curve around Γ for the lower band as shown in the top left panel. Between two contour curves, Ω is slightly negative. Ω is positive outside the outer contour curve as shown in the top left panel of Fig. 2(b), but significant non-zero Ω occurs only around K and K' . In the region of $\Delta_c > 0$ and $-\Delta_c < \Delta < \Delta_c$, the upper

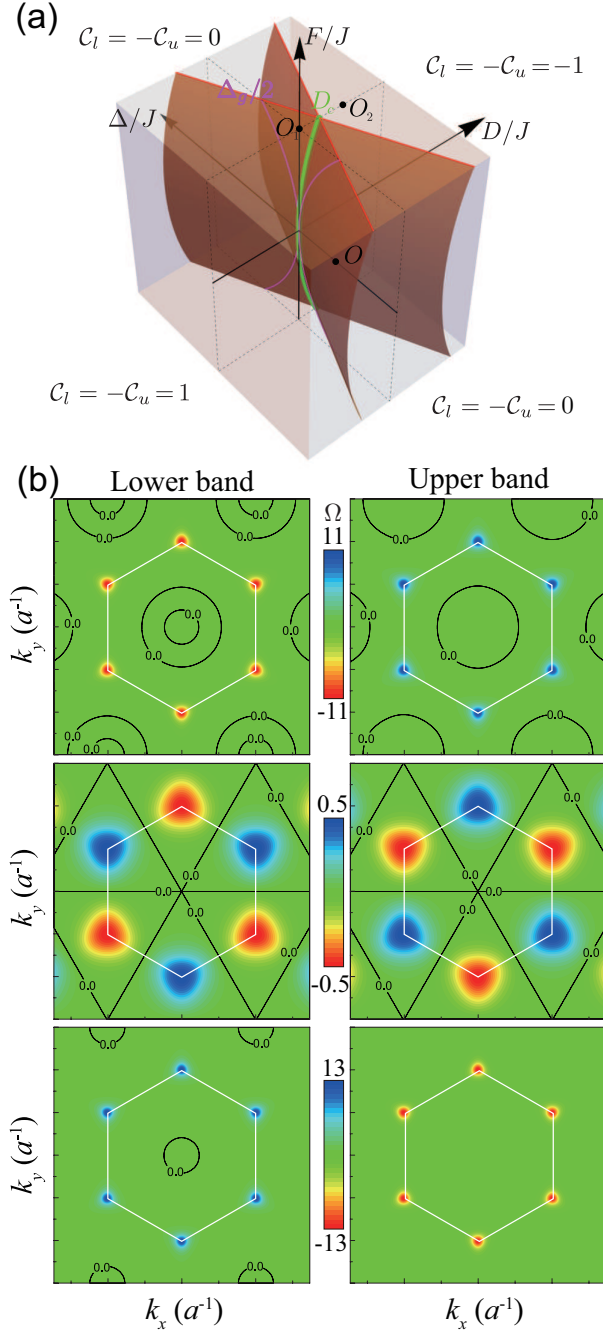


FIG. 2. (a) Phase diagram in $D/J - \Delta/J - F/J$ space for $K = 10J$. Phases are classified by the Chern numbers of the upper and lower magnon bands. Three phases of $C_l = -C_u = 1$; $C_l = -C_u = -1$; and $C_l = C_u = 0$ are separated by two orange boundary surfaces. The green line, $D = \frac{\sqrt{3}F^2}{16M}$ and $\Delta = 0$, is the intersection of the two boundary surfaces. The magenta lines, $\Delta = \pm \Delta_g/2$ and $D = 0$, are the intersections of the boundary surfaces with the $D = 0$ plane. O_1 ($F = 5J$, $D = \Delta = 0$), O_2 ($F = 5J$, $D = 0.4J$, $\Delta = 0$), and O ($F = D = 0$, $\Delta = -1.5J$) are 3 representative points in topologically nontrivial phase of $C_l = -C_u = -1$; $C_l = -C_u = 1$, and topologically trivial phase $C_l = C_u = 0$, respectively. (b) The z component of Berry curvature $\Omega = \mathbf{\Omega} \cdot \hat{\mathbf{z}}$ for O_1 , O , O_2 (from top to bottom). The left panel is for the lower magnon band and

magnon band has Chern number -1 . The bottom panel of Fig. 2(b) is the density plot of Ω of lower (left panel) and upper (right panel) bands for a representative point of $F = 5J$, $\Delta = 0$, $D = 0.4J$ (O_2 in Fig. 2(a)) in this topologically nontrivial phase. The lower band has only one contour curve of $\Omega = 0$ (black dash curve) around Γ that divides the first Brillouin zone into two parts. Inside the contour curve, Ω is slightly positive as shown in the bottom left panel of Fig. 2(b). It is negative outside the contour curve with significant non-zero value around K and K' . The system is in topologically trivial phase for both lower and upper bands in the other two regions. Ω around K and K' valleys have opposite sign so that the Chern numbers are 0 for both bands. We consider O in Fig. 2(a) ($F = D = 0$, $\Delta = 1.5J$) as a representative point in the phase. The middle panel of Fig. 2(b) shows the density plot of Ω at O for the two bands. Indeed, Berry curvatures Ω at K and K' have opposite value, and Chern numbers are zeros. For $\Delta = 0$, the band gaps at K and K' close and reopen at the same time and the Chern number of the upper band changes from -1 to $+1$ if we tune the DMI crossing the line of $D = \frac{\sqrt{3}F^2}{16M}$ and $\Delta = 0$ [the green line in Figure 2(a)]. The system changes from one topologically nontrivial phase to another. The features of the phase diagram discussed above preserves as long as system ground state is the perpendicular ferromagnetic state.

Let us consider the magnon transport in an infinite system. Apply a thermal gradient along x direction, the motion of a magnon wavepacket is governed by the semiclassical equations [11, 18],

$$\dot{\mathbf{r}} = \frac{1}{\hbar} \frac{\partial \varepsilon}{\partial \mathbf{k}} - \dot{\mathbf{k}} \times \boldsymbol{\Omega}; \quad (10)$$

$$\dot{\mathbf{k}} = \frac{1}{\hbar} \mathbf{F} = -\frac{1}{\hbar} \frac{\partial \varepsilon}{\partial \mathbf{r}} + \frac{q}{\hbar} \dot{\mathbf{r}} \times \mathbf{B}, \quad (11)$$

Where $\varepsilon(\mathbf{r}, \mathbf{k}) = \hbar\omega(\mathbf{k}) + \phi(\mathbf{r})$ is the energy of the magnon with $\phi(\mathbf{r})$ being the potential energy, and \mathbf{F} is the total force on the magnon. q is the charge of the particle and $q = 0$ for a magnon. In the presence of a thermal gradient, the Boltzmann equation of the magnon is

$$\dot{\mathbf{r}} \cdot \frac{\partial f}{\partial \mathbf{r}} = -\frac{f - f_0}{\tau} \equiv -\frac{f_1}{\tau}, \quad (12)$$

where $f(\mathbf{r}, \mathbf{k})$ is the magnon distribution function. $f_0 = 1/(e^{\beta\hbar\omega} - 1)$ is the Bose-Einstein distribution of zero chemical potential at local temperature T [$\beta = (k_B T)^{-1}$]. τ is magnon relaxation time. f_1 is the deviation of the distribution function from its equilibrium values. In the linear response regime where the thermal gradient is small, Eq. (12) can be written

as

$$\dot{\mathbf{r}} \cdot \frac{\partial f_0}{\partial \mathbf{r}} = -\frac{f_1}{\tau}. \quad (13)$$

One can prove the following identity,

$$\dot{\mathbf{r}} \cdot \frac{\partial f_0}{\partial \mathbf{r}} = \left(-\frac{\hbar\omega}{T} \nabla T \right) \cdot \frac{\partial f_0}{\hbar \partial \mathbf{k}}. \quad (14)$$

Substituting Eq. (14) into the left hand side of Eq. (13), it yields

$$\left(-\frac{\hbar\omega}{T} \nabla T \right) \cdot \frac{\partial f_0}{\hbar \partial \mathbf{k}} = -\frac{f_1}{\tau}. \quad (15)$$

Thus, one can identify a thermal force $\mathbf{F}_T = \left(-\frac{\hbar\omega}{T} \nabla T \right)$ proportional to the magnon frequency and the thermal gradient [19]. Insert (11) into (10) with $\mathbf{F} = \mathbf{F}_T$, we obtain

$$\dot{\mathbf{r}} = \frac{\partial \omega}{\partial \mathbf{k}} + \frac{\omega}{T} \nabla T \times \boldsymbol{\Omega}. \quad (16)$$

The magnon current density is given by $\mathbf{j}_m = \sum_{n,\mathbf{k}} [\dot{\mathbf{r}} f(n, \mathbf{k})]$, where the summation is over all magnon states. Keep terms linear in the thermal gradient and convert the summation to integration, we have

$$\mathbf{j}_m = \overleftrightarrow{\boldsymbol{\kappa}} (-k_B \nabla T), \quad (17)$$

where the longitudinal heat conductance κ_{xx} and the anomalous Nernst coefficient κ_{xy} are

$$\kappa_{xx} = \frac{\tau}{(2\pi)^2} \sum_n \iint \beta \left(\frac{\partial \omega_n}{\partial k_x} \right)^2 \rho(\beta \hbar \omega_n) d^2 \mathbf{k}, \quad (18)$$

$$\kappa_{xy} = \frac{1}{(2\pi)^2} \sum_n \iint \beta \omega_n \Omega_n f_0(\beta \hbar \omega_n) d^2 \mathbf{k}, \quad (19)$$

where $\rho(x) = \frac{x e^x}{(e^x - 1)^2}$, $f_0(x) = \frac{1}{e^x - 1}$, and $n = 1, 2$ labels the lower and upper magnon bands. Figure 3(a) shows the temperature dependence of κ_{xx} and κ_{xy} in two different topologically-nontrivial phases specified by O_1 and O_2 in Fig. 2(a). In order to have a quantitative feeling about the results, we use Sr_2IrO_4 parameters of $a = 0.55$ nm [20], $J = 19.6 \mu_0 \mu_B^2 / a^3$ [10], and $\gamma = 2.21 \times 10^5$ rad/s/(A/m) in all the following discussions. The longitudinal heat conductance κ_{xx} is always positive as expected from thermodynamic laws that the magnons move from the hot side to the cold side. Eq. (19) says that the AMNE coefficient is determined by the Berry curvature distribution in the momentum space and the magnon equilibrium distribution function. Since magnon number in the lower band is bigger than that in the higher band according to the Bose-Einstein distribution, the sign of AMNE

coefficient is always determined by the Berry curvature of the lower magnon band. At very low temperature, only the magnons near Γ point [band bottom (top) of the lower (upper) band] are excited. The sign of AMNE coefficient is determined by Ω around Γ , and its value is small because Berry curvature Ω is very close to zero, if not exactly zero, and the magnon number is also small there. At a higher temperature when the magnon number near K and K' points [band top (bottom) of the lower (lower) band] are large enough and dominate the AMNE due to significant non-zero values of the Berry curvature only near there. At even higher temperature when equal-partition theorem become true so that $f_0 \approx k_B T / (\hbar \omega)$, the AMNE coefficient is close to zero because κ_{xy} is approximately proportional to $(\mathcal{C}_u + \mathcal{C}_l) = 0$ [15, 17], i.e. the contributions from two bands cancel with each other.

The general behavior of AMNE coefficient κ_{xy} mentioned above can be illustrated by two representative points in two distinct topologically nontrivial phases of $C_l = -1$ (for O_1) and $C_l = 1$ (for O_2). For O_1 whose Berry curvature distribution is given in the top panel of Fig. 2(b), κ_{xy} is always positive, a transverse magnon current along $\mathbf{m}_0 \times (-\nabla T)$, because Ω are positive near both Γ and K (K') points. For O_2 , at very low temperatures when the magnon number around K and K' are negligible and only the magnons near Γ point are excited, κ_{xy} decreases and becomes more and more negative initially with the increase of temperature because Ω is negative near Γ point. However, when magnons near K and K' points are excited, κ_{xy} starts to increase with temperature, and becomes positive after an intermediate temperature because Ω has large positive values near K and K' . Thus, in this phase the sign of the AMNE coefficient reverses at the intermediate temperature. The numerical results of κ_{xx} and κ_{xy} at higher temperature are shown in the inset of Figure 3(a). The longitudinal heat conductance κ_{xx} saturates at high temperature. AMNE coefficient κ_{xy} at O_1 (O_2) increases from 0 to a maximum positive (negative) value as the temperature increases, and then gradually go back to 0 when magnons in the upper band are thermally excited. This indicates that there is an optimal temperature for the maximal AMNE coefficient. If this temperature does not exceed the Curie temperature, it should be used for the largest AMNE.

In the topologically trivial phase, the Berry curvatures Ω Of the same band has opposite values near K and K' points. Thus the contributions to AMNE from different valleys cancel each other, and the net transverse magnon current can be in either direction, depending on the parameters. Figure 3(b) is the density plots of κ_{xy} as a function of D/J and Δ/J at different temperatures (for $K = 10J$ and $F = 5J$). Because of the featured distribution

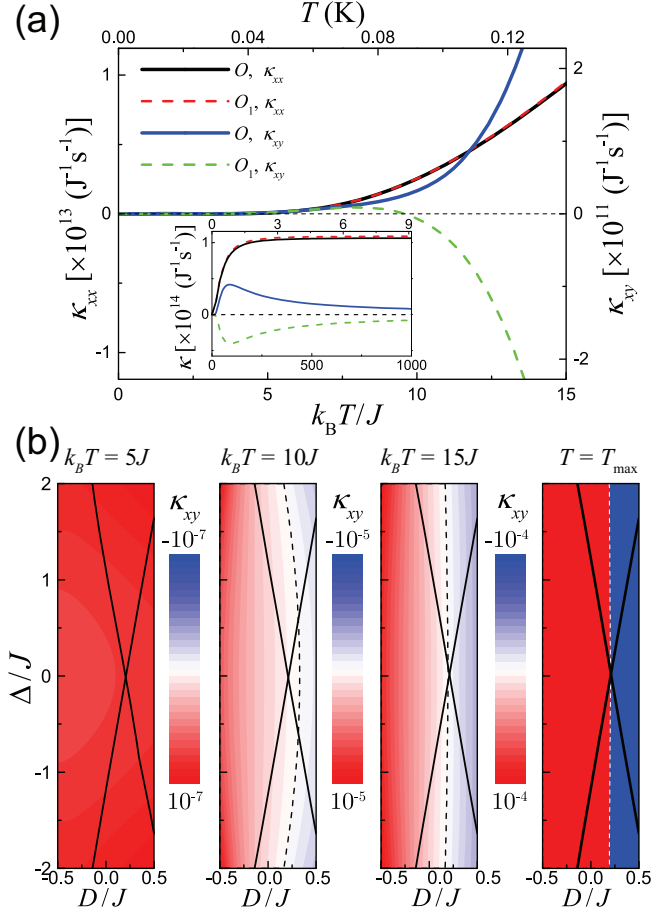


FIG. 3. (a) The longitudinal magnon conductance κ_{xx} (left axis) and AMNE coefficient κ_{xy} (right axis) for parameters at O_1 and O_2 . The inset shows the high-temperature values of the same quantities. (b) (Panels 1 to 3) The density plots of κ_{xy} [in units of $\text{eV}^{-1}\text{s}^{-1}$] in D/J - Δ/J plane for $K = 10J$ and $F = 5J$ at different temperatures. The black solid lines are topological phase boundaries, and the black dashed lines are the contour lines of $\kappa_{xy} = 0$. WHY COLOR BARS are negative on top and po on bot.? What are the use of black lines? (Panel 4) The sign of the maximum value of κ_{xy} . Red region is for positive κ_{xy} and blue region is for negative κ_{xy} . The dashed line is the contour curve of $\kappa_{xy} = 0$.

of Berry curvature near Γ discussed above, the sign change of κ_{xy} happens at larger D at lower temperatures, and is different to the topological phase boundaries as shown by the black solid lines. However, the sign change of κ_{xy} is closely related to the topological phase transition, as shown in the last panel of Figure 3(b). The sign change of κ_{xy} coincides with the topological phase transition line of $D = \frac{\sqrt{3}F^2}{16M}$ and $\Delta = 0$. Tuning the DMI can drive

the system from one topologically nontrivial phase to another at $\Delta = 0$. The sign change of κ_{xy} at the maximum point changes at the same time due to the sign-reversal of Berry curvatures. This also means for the parameters of negative κ_{xy} in the last panel, there is a temperature-induced sign reversal of κ_{xy} .

In the above discussions, we studied the magnon Nernst effect, a transverse magnon current generated by a longitudinal thermal gradient. Similar to electronic systems, there are other related effects, such as a transverse magnon current induced by a longitudinal chemical potential gradient (magnon Hall effect and anomalous magnon Hall effect), and a transverse magnon heat current induced by a longitudinal chemical potential gradient (magnon Peltier effect). These effects can be investigated in the same way as what have done here for the same Berry curvature physics. Similar topological phase transitions and sign-reversal of AMNE was also predicted in pyrochlore lattices [21]. In the calculation of thermal transport coefficients, the thermal energy $k_B T$ is allowed to be much higher than J . In real materials, the temperature is limited by the Curie temperature that is order of J/k_B . For example, $J = 20$ meV ($2.5 \times 10^5 \mu_0 \mu^2 / a^3$) and the Curie temperature is about 240 K [22] for Sr_2IrO_4 . The sign-reversal temperature is $9.5J/k_B$ as shown in Figure 3(a). Thus, the temperature is much smaller than the sign-reversal temperature in this case so the AMNE coefficient should be always positive. The reason why the Berry curvature near Γ point has opposite sign, and the factors that affect the Berry curvature distribution are still open questions.

III. CONCLUSION

In conclusion, we studied the thermal magnon transport of perpendicularly magnetized honeycomb lattice with the nearest-neighbor pseudodipolar interaction and the next-nearest-neighbor DMI. We show that the system has various topological nontrivial phases. Due to the nontrivial Berry curvature, a transverse magnon current appears when a thermal gradient is applied, resulting in an anomalous Magnon Nernst effect. The sign of the anomalous Magnon Nernst effect is reversed by tuning DMI and temperature.

ACKNOWLEDGEMENTS

This work was supported by National Natural Science Foundation of China (Grant No. 11374249) and Hong Kong RGC (Grant No. 16300117 and 16301816). X.S.W acknowledge support from UESTC and China Postdoctoral Science Foundation (Grant No. 2017M612932).

REFERENCE

- [1] Žutić I, Fabian J and Das Sarma S 2004 *Rev. Mod. Phys.* **76** 323
- [2] Wang X S, Yan P, Shen Y H, Bauer G E W and Wang X R 2012 *Phys. Rev. Lett.* **109** 167209
- [3] Hu B and Wang X R 2013 *Phys. Rev. Lett.* **111** 027205
- [4] Demokritov S O and Slavin A N 2013 *Magnonics: From Fundamentals to Applications* (Springer, Topics in Applied Physics Vol. 125)
- [5] Kruglyak V V , Demokritov S O and Grundler D 2010 *J. Phys. D: Appl. Phys.* **43** 264001
- [6] Serga A A, Chumak A V and Hillebrands B 2010 *J. Phys. D: Appl. Phys.* **43** 264002
- [7] Nagaosa N, Sinova J, Onoda S, MacDonald A H and Ong N P 2010 *Rev. Mod. Phys.* **82** 1539
- [8] Wang X S, Su Y and Wang X R 2017 *Phys. Rev. B* **95** 014435
- [9] Moriya T 1960 *Phys. Rev.* **120** 91
- [10] Jackeli G and Khaliullin G 2009 *Phys. Rev. Lett.* **102** 017205
- [11] Matsumoto R and Murakami S 2011 *Phys. Rev. Lett.* **106** 197202
- [12] Gilbert T L 2004 *IEEE. Trans. Magn.* **40** 3443
- [13] Wang X S, Zhang H W and Wang X R arXiv:1706.09548
- [14] White R M, Sparks M and Ortenburger I 1965 *Phys. Rev.* **139**, A450
- [15] Avron J E, Seiler R and Simon B 1983 *Phys. Rev. Lett.* **51**, 51
- [16] Shindou R, Matsumoto R, Murakami S and Ohe J I 2013 *Phys. Rev. B* **87** 174427
- [17] Bohm A, Mostafazadeh A, Koizumi H, Niu Q and Zwanziger J 2003 *The Geometric Phase in Quantum Systems: Foundations, Mathematical Concepts, and Applications in Molecular and Condensed Matter Physics* (Springer, Berlin).

- [18] Xiao D, Chang M -C and Niu Q 2010 *Rev. Mod. Phys.* **82** 1959
- [19] Luttinger J M 1964 *Phys. Rev.* **135** A1505
- [20] Huang Q, Soubeyroux J L, Chmaissem O, Natali Sora I, Santoro A, Cava R J, Krajewski J J and Peck W F Jr 1994 *J. Solid State Chem.* **112**, 355
- [21] Mook A, Henk J and Mertig I 2014 *Phys. Rev. B* **89** 134409
- [22] Kim J, Casa D, Upton M H, Gog T, Kim Y -J, Mitchell J F, van Veenendaal M, Daghofer M, van den Brink J, Khaliullin G and Kim B J 2012 *Phys. Rev. Lett.* **108** 177003